SAN096-1717C

ENERGETIC-PARTICLE SYNTHESIS OF NANOCOMPOSITE Al ALLOYS

D. M. FOLLSTAEDT, J. A. KNAPP, J. C. BARBOUR, S. M. MYERS and M. T. DUGGER
Sandia National Laboratories, Albuquerque, NM 87185-1056 (dmfolls@sandia.gov)

ABSTRACT

Ion implantation of O into Al and growth of Al(O) layers using electron-cyclotron resonance plasma and pulsed laser depositions produce composite alloys with a high density of nanometer-size oxide precipitates in an Al matrix. The precipitates impart high strength to the alloy and reduced adhesion during sliding contact, while electrical conductivity and ductility are retained. Implantation of N into Al produces similar microstructures and mechanical properties. The athermal energies of deposited atoms are a key factor in achieving these properties.

INTRODUCTION

Energetic atoms can often be used to form alloy layers with properties superior to those of alloys formed by purely thermal methods. Ion implantation can introduce essentially any species up to high concentrations (10's of atomic percent) in any substrate, independently of its solid solubility. Energetic particles can not only overcome such thermodynamic limitations, but can also alter the microstructure by displacing atoms in the alloy with their kinetic energy before coming to rest. Implantation can thus form surface alloys that are supersaturated solid solutions, amorphous phases, or densely precipitated layers. Similar processes occur during the deposition of alloy layers using isolated, energetic atoms.

Here we consider synthesis of precipitation-hardened Al(O) alloy layers by implantation of O^+ into Al and by two methods using athermal deposition of atoms: electron-cyclotron resonance (ECR) plasma deposition and pulsed-laser deposition (PLD). Each method produces a high density of nanometer-size oxide precipitates in an Al matrix. Such structures are rather ideal nanocomposites since the dispersed precipitates impart exceptional mechanical properties to the alloy layer while it retains key metallic properties of the matrix. We demonstrate the microstructure of O-implanted Al and discuss its strength and tribological properties in terms of precipitation hardening. The PLD and ECR alloy layers deposited on Si are shown to have similar microstructures, and electrical conductivity and ductility are shown to be metal-like for these alloys. Examination of N-implanted Al shows similar fine precipitates and enhanced mechanical properties. We discuss key features of alloy systems and energetic-particle synthesis that allow such desirable microstructures to be formed.

SYNTHESIS AND EVALUATION OF Al(O) ALLOY LAYERS

Ion implantation of O^+ into well-annealed Al with several energies from 25 to 200 keV was used to form alloys with a nearly constant composition extending ~0.5 μm deep [1]. The microstructures were evaluated with transmission electron microscopy (TEM), as seen in Fig. 1a for 17 at.% O [2]. The electron diffraction pattern demonstrates that when the fcc Al matrix is tilted a few degrees off a zone axis, there is a diffuse oxide reflection under each weakened Al reflection; detailed considerations indicate that the phase is γ-Al_2O_3. This phase (cubic spinel, $a_o = 0.790$ nm) precipitates instead of the equilibrium hexagonal phase (corundum), apparently because its atomic spacings closely match those of the Al matrix. Dark-field imaging with a diffuse reflection illuminates a high density of precipitates 1.5 - 3.5 nm in diameter that appear

DISCLAIMER

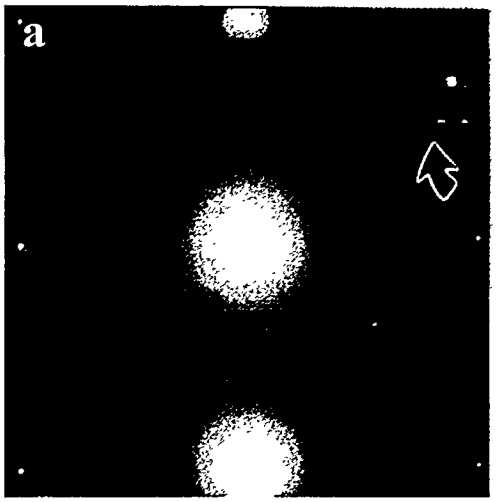

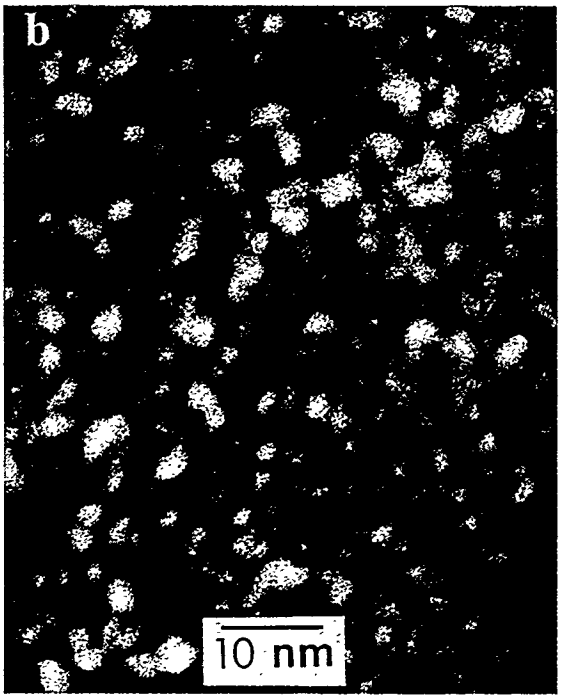

Figure 1. a) Electron diffraction pattern for O-implanted $Al_{83}O_{17}$ alloy with the Al matrix tilted off the [100] zone axis to show diffuse γ-Al_2O_3 reflections. b) Dark-field image of precipitates, obtained with a diffuse reflection.

randomly dispersed and isolated from one another; see Fig. 1b. Their small size and lattice matching together imply that the precipitates are coherent with the Al matrix.

Several features of the Al-O alloy system appear responsible for the high density of small precipitates. These two elements react very exothermically with one another, giving O a very low solid solubility in Al, $<3x10^{-8}$ at.% [3]. Further, each atom in the material is calculated to have been displaced many times, producing numerous point defects that provide nucleation sites for the oxide. The displacements and mobility of point defects in Al at room temperature probably also provide the mobility for O atoms to migrate and attach to precipitates.

The strengths of the Al(O) alloy layers are probed with ultra-low load "nanoindentation" to depths partially through the layer. Figure 2a shows the load response of Al implanted with 10 at.% O to indentation to 150 nm depth. Finite-element modeling was used to evaluate the mechanical properties of the alloy by using the known properties of the substrate and adjusting the properties of the layer to fit this experimental load versus depth response. The model divides the diamond tip, alloy layer and substrate into elements as in Fig. 2b, and their deformation during indentation is computed while maintaining contact with neighboring elements. The unloading portion of the curve is also shown in Fig. 2a; its initial slope at maximum depth is an elastic response that is used to evaluate Young's modulus. The loading portion of the curve depends on both Young's modulus and the yield stress. Finite-element modeling is essential to obtaining accurate properties for the layer because the observed response is due to the layer/substrate combination. For Al(O) layers on well-annealed Al, the response is softened by the substrate (yield stress = 0.041 GPa). The simulation in Fig. 2a was obtained with the commercial code ABAQUS [4] and fits the loading curve and unloading slope well with 2.4 ± 0.12 GPa for yield stress and 135 ± 7 GPa for Young's modulus of the alloy. Tests of implanted alloys with 5 - 20 at.% O give yield stresses of 1.4-2.9 GPa [1], much higher than for commercial Al alloys and like high-strength steels. The absolute error in evaluating these properties is judged to be < 20%.

The exceptional strength of O-implanted Al is due to the high density of hard precipitates. When their size and density are used in conventional dispersion hardening theory, good agree-

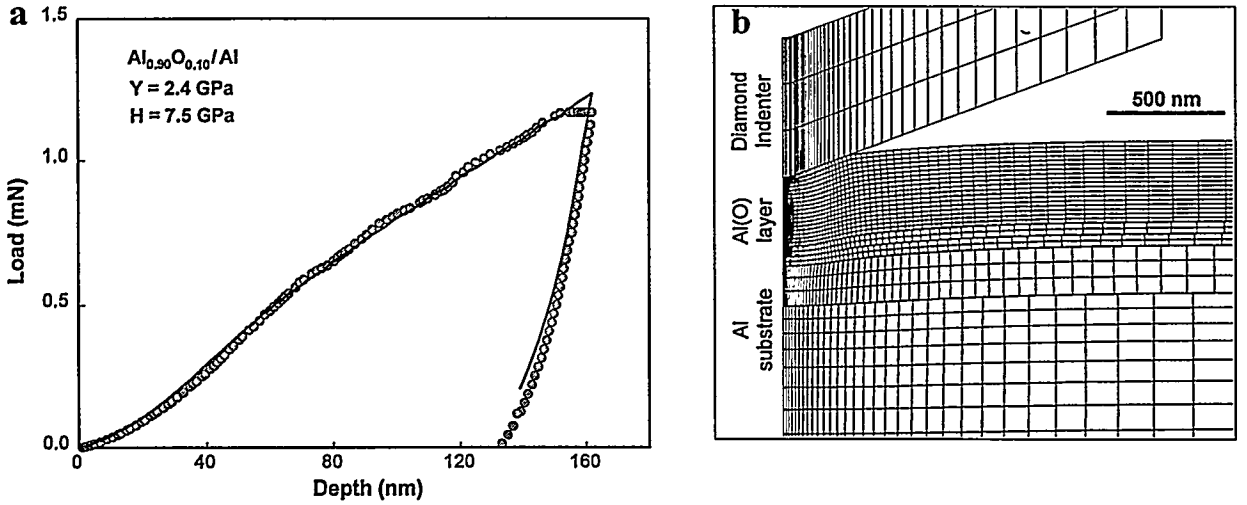

Figure 2. a) Nanoindentation load versus depth data (points) for Al implanted with 10 at.% O and simulation (curve) using a yield stress of 2.4 GPa. b) Mesh used for finite-element simulation in a).

ment is obtained with the magnitude and composition variation of the alloy strength [1]. Thus the mechanical properties are those of Al with a high density of particles blocking dislocation motion.

Implantation of O significantly improves the tribological properties of Al [1,5]. Whereas untreated Al shows "stick-slip" adhesion during pin-on-disk testing, implantation of as little as 5 at.% O eliminates it and changes the wear to a mild abrasive mode with a coefficient of friction of ~0.2. Benefits persist for several tens of cycles until the layer is worn through and stick-slip occurs. The reduced friction and wear are believed due to the high strength of the O-implanted surface layer since the strong material deforms less under the loaded pin and the contact area for adhesion is reduced correspondingly.

To form thicker Al(O) alloys, Al is evaporated onto a Si substrate with O_2^+ ions simultaneously incident from the ECR plasma source. These ions stream from the source with an energy of 30 eV, but the energy can be increased by biasing the specimen up to -300 V. The O atoms are

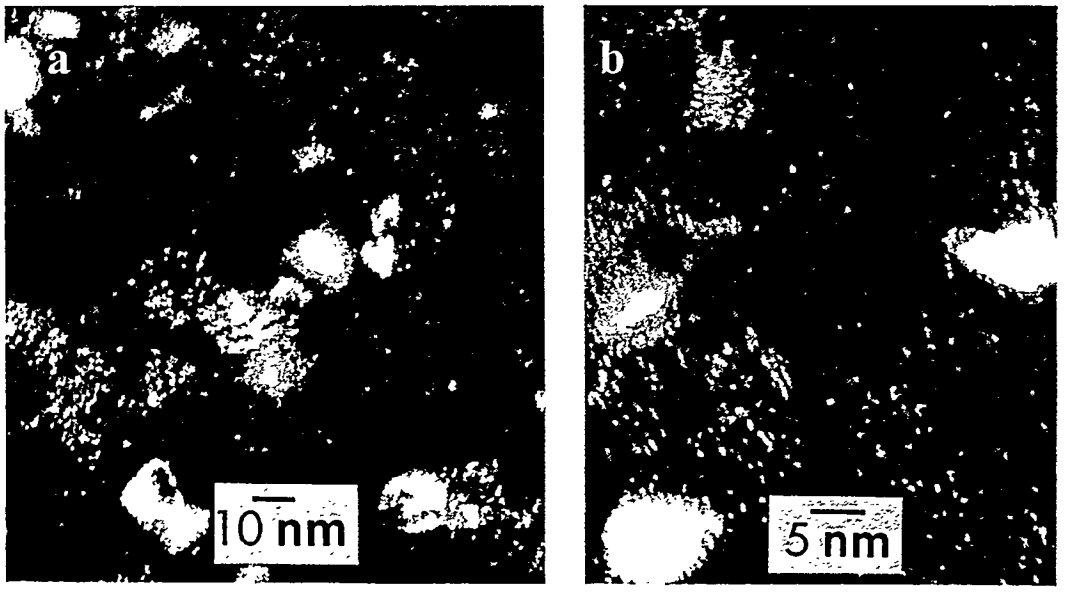

Figure 3. Dark-field images showing Al grains (larger white areas) and oxide precipitates (fine white spots) in a) ECR-synthesized $Al_{74}O_{26}$ and b) PLD-synthesized $Al_{69}O_{31}$ (greater magnification).

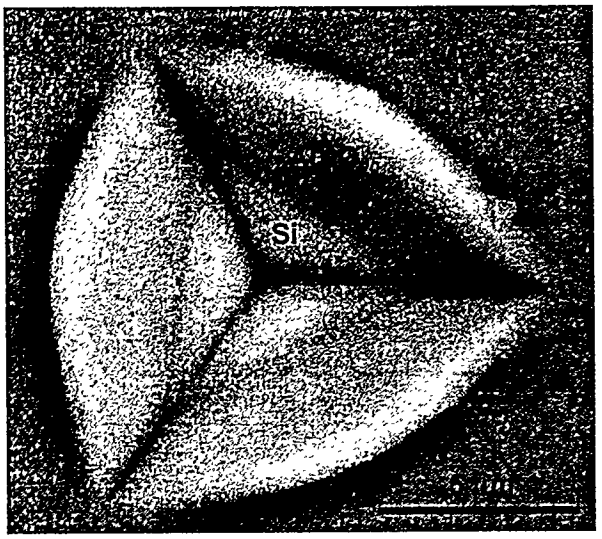

Figure 4. Secondary electron image of 1 μm-deep indent of PLD $Al_{80}O_{20}$ alloy layer on Si.

calculated to penetrate the surface by 1.5-3.5 nm and to displace atoms in the growing layer. In these features, ECR synthesis is similar to high energy implantation, but the O_2^+ are implanted into a growing layer that can be micrometers thick. Dark-field imaging of an $Al_{74}O_{26}$ alloy layer shows fine grains of fcc Al (12 - 80 nm) with 1-2 nm oxide precipitates within the grains, as indicated in Fig. 3a. Indentation and modeling of ECR layers deposited near 100°C gives yield stresses of 0.62 - 1.3 GPa for 9 - 20 at.% O. This synthesis thus produces a microstructure similar to that for implantation and strengths that are high, although less than those of ion-implanted alloys of the same O concentration. The reduction in strength is not yet understood, but it is possible that deposited layers are not as fully dense as implanted layers.

Alloy layers of Al(O) can also be deposited with PLD by sequentially ablating Al and Al_2O_3 targets [6]. Composition is determined by the ratio of pulses per target, and the amount of material deposited per cycle is kept at ~1 monolayer to achieve a near-homogeneous deposition. The energies of atoms in the laser-ablated plasma plume are ~10 eV, which is insufficient to penetrate into the layer. However, the atoms reach the specimen with greater energies several hundred times k_BT (0.025 eV) and may thermally break surface bonds or directly displace surface atoms, which are less strongly bound. The dark-field image in Fig. 3b shows a microstructure of 5 - 25 nm fcc Al grains with ~1 nm oxides, similar to that with ECR but on a finer scale. The strengths of PLD alloys with 20 and 29 at.% O are 1.7 and 2.5 GPa, respectively [6], which are higher than for corresponding ECR alloys but below implanted alloys. Thus this relatively low energy deposition method also produces a nanocomposite microstructure with high yield stress.

The ECR and PLD layers allow us to examine two properties of the precipitated alloy layers. First, the electrical resistivities of ECR alloys deposited at 200°C with 27 at.% O and an evaporated pure Al layer were examined with a four-point probe. The alloy values of 65 - 89 μΩ-cm are significantly increased from that of the pure Al layer, 2.5 μΩ-cm, but are nonetheless metal-like and similar those of metal silicides. Electron scattering from the oxides apparently increases the resistivity, but the Al matrix is still significantly conductive. Second, the ductility of Al(O) is demonstrated in Fig. 4 by indentation through a 340 nm $Al_{80}O_{20}$ PLD layer and into the Si substrate to 1 μm total depth; the alloy/substrate interface can be seen. The alloy overlayer is smoothly displaced to the sides of the indent, but remains attached to the substrate and shows no evidence of fracture. Thus two key properties of metals are retained in our Al(O) with up to ~30 vol.% oxide, which is consistent with the continuous metal matrix and isolated precipitates.

EVALUATION OF N-IMPLANTED Al ALLOY LAYERS

We have recently examined N implantation of Al to determine whether high-strength alloys are produced and to compare alloy properties to those of Al(O). Precipitation of hexagonal AlN was expected, which could provide insight into the blocking of dislocations because the crystal

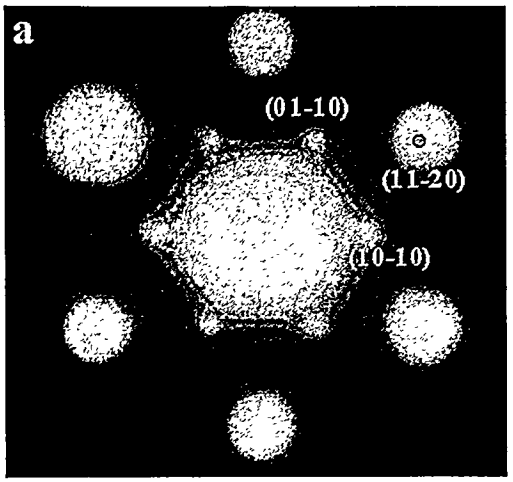

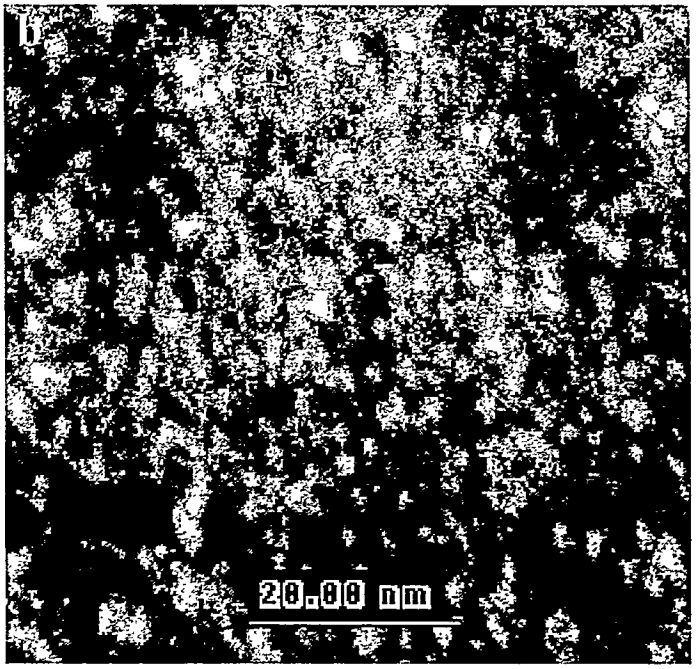

Figure 5. a) [111] diffraction pattern from Al implanted with 10 at.% N, showing weak AlN reflections (indexed), and b) dark-field image of AlN precipitates.

structure of AlN differs from that of cubic γ-Al_2O_3 and its bonds are more covalent. Annealed Al was implanted with 10 at.% N at room temperature and examined with TEM. Electron diffraction patterns show extra spots matching reflections of AlN, which align in the pattern of intense fcc Al reflections as in Fig. 5a. The precipitates align with the c-axis along a <111> matrix direction and with their {1-100} planes parallel to {2-20} Al planes. Dark-field imaging with these reflections shows precipitates ~2 nm in diameter as seen in Fig. 5b.

Nanoindentation was done on a specimen implanted with 5 at.% N to a depth of 0.5 μm, and the response curve is shown in Fig. 6. For loads $\leq$ 0.4 mN (depths $\leq$ 70 nm) the alloy layer appears quite strong; finite-element simulation using a yield stress of 2.15 GPa is seen to fit this portion of the curve well. However at higher loads, abrupt penetrations to greater depth are seen, termed "pop-ins" [7]. The origin of these features is not yet clear for N-implanted Al; they were not observed in O-implanted Al. Considering the initial part of the curve only, the $Al_{95}N_5$ alloy layer appears stronger than the corresponding $Al_{95}O_5$ alloy with yield stress = 1.4 GPa.

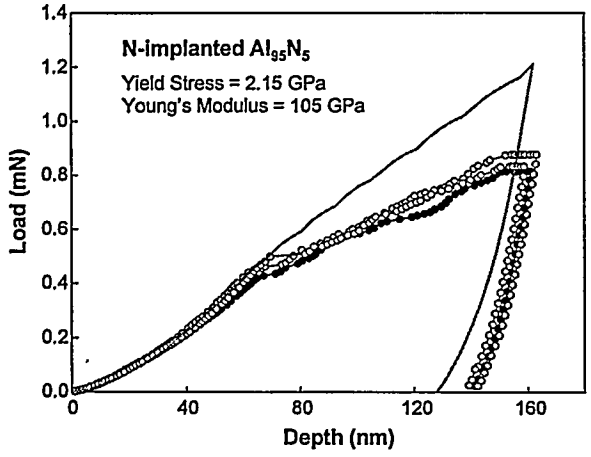

Figure 6. Nanoindentation of $Al_{95}N_5$ and fit to low-load portion using indicated alloy parameters.

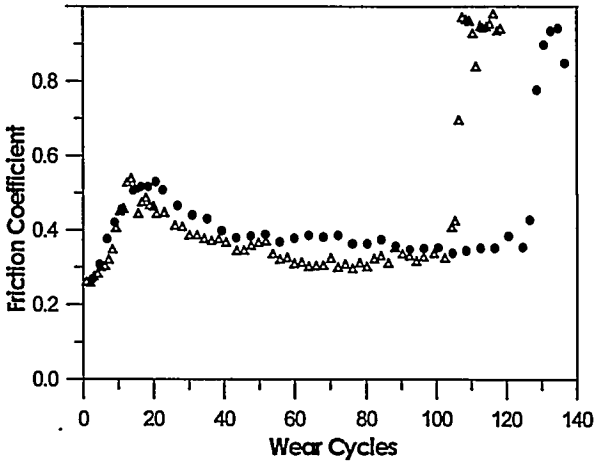

Figure 7. Friction coefficient versus wear cycles for N-implanted $Al_{95}N_5$.

The coefficients of friction obtained with a reciprocating tester for two tests of the $Al_{95}N_5$ alloy layer are shown in Fig. 7. The implantation has again eliminated stick-slip adhesion, and after a maximum at ~15 cycles the coefficient stabilizes at ~0.35 where it persists for over 100 cycles. Eventually, the implanted layer appears to be worn through and the adhesion returns (coefficient of friction approaches 1). This behavior is like that of O-implanted Al, but the benefits with only 5 at.% N appear to persist longer. The difference in steady-state coefficient of friction from earlier work with O implantation (~0.2) [4] is not yet understood.

CONCLUSIONS

By introducing insoluble species as individual energetic atoms into a metal matrix, nanocomposite structures can be formed with ion implantation. The numerous lattice defects created by the process provide a high density of nucleation sites, leading to nanometer-scale precipitate microstructures. This microstructural refinement is perhaps more extreme for Al(O) because of the high reactivity of the two elements. The ECR and PLD plasma syntheses using atoms with lower energies produce similar composite microstructures of 1-2 nm oxides within their small Al grains ($\lesssim$ 100 nm). The high density of isolated precipitates strengthens Al to the level of high-strength steels and reduces adhesion during dry sliding contact, while retaining electrical conductivity and ductility through the metal matrix. Implantation of N also produces a high density of fine precipitates in Al, and is very effective for strengthening and reducing adhesion during sliding contact. The indentation of N-implanted Al requires more study to understand "pop-in" abrupt yielding events.

ACKNOWLEDGEMENTS

The authors wish to thank G. A. Petersen for performing ion implantations, M. P. Moran for assistance with TEM examinations, and L. Sorroche for tribological testing. This work was supported by the United States Department of Energy under Contract DE-AC04-94Al85000, in part by its Office of Basic Energy Sciences and the Center of Excellence for Synthesis and Processing of Materials. Sandia is a multiprogram laboratory operated by Sandia Corporation, a Lockheed Martin Company, for the United States Department of Energy.

REFERENCES

1. D. M. Follstaedt, S. M. Myers, R. J. Bourcier and M. T. Dugger, "Proc. Intl. Conf. On Beam Processing of Advanced Materials", eds. J. Singh and S. M. Copley (TMS, Warrendale, PA, 1993), pp.507.
2. D. M. Follstaedt, S. M. Myers and R. J. Bourcier, Nucl. Inst. Meth. **B59/60**, 909 (1991).
3. "Binary Alloy Phase Diagrams", eds. T. B. Massalski, J. L. Murray, L. H. Bennett and H. Baker (ASM International, Metals Park, OH, 1986), Vol. 1, p. 143.
4. ABAQUS/Standard v.5.5, Hibbitt, Karlsson & Sorensen, Inc., Pawtucket, RI.
5. M. T. Dugger, R. J. Bourcier, D. M. Follstaedt and S. M. Myers, Tribology International, in press.
6. J. A. Knapp, D. M. Follstaedt and S. M. Myers, J. Appl. Phys. **79**, 1116 (1996). The high yield stress reported in this paper for $Al_{80}O_{20}$ (5.1 GPa) is in error due to incorrect indentation; the correct value is 1.7 GPa. The value for $Al_{71}O_{29}$ has changed slightly to 2.5 GPa due to refinements in the modeling.
7. A. B. Mann, J. B. Pethica, W. D. Nix and S. Tomiya, Mat. Res. Soc. Symp. Proc. **356**, 271 (1995).